

Supporting Information

Structure and Assembly Mechanism of a Centipede-shaped High-nuclear Dy₁₄Cu₁₂ Heterometallic Nanocluster

Shui Yu,^{a,b} Huancheng Hu,^{*a} Zhihui Qiu,^{*a} Yuzhen Zhang,^c Dongcheng Liu,^a Yunying Liang,^a Hua-Hong Zou,^a Fu-Pei Liang,^{ad} Zilu Chen^{*a}

^a State Key Laboratory for Chemistry and Molecular Engineering of Medicinal Resources, School of Chemistry and Pharmaceutical Sciences, Guangxi Normal University, Guilin 541004, China. E-mail: siniantongnian@126.com, zhihuiqiu@aliyun.com, zlchen@mailbox.gxnu.edu.cn

^b School of Pharmacy, Binzhou Medical University, Yantai 264003, PR China.

^c School of Chemistry and Chemical Engineering, Guangxi Minzu University, No. 158, Daxue West Road, Nanning, Guangxi 530006, China.

^d Guangxi Key Laboratory of Electrochemical and Magnetochemical Functional Materials, College of Chemistry and Bioengineering, Guilin University of Technology, Guilin, 541004, P.R. China.

Table of Contents

1. Experimental	2
2. Continuous shape measure calculation results for Dy(III) ions.....	5
3. Crystallographic data, bond distances and angles	8
4. IR, PXRD and TG figures of 1	12
5. Additional structural figures of 1	13
6. Major species and fragments detected in 1	15
7. The superposed simulated and observed spectra of several species figure of 1	17
8. Additional figures for static magnetic properties of 1	20

1. Experimental

Materials and Measurements

All chemical reagents were used as commercially received without further purification. The Fourier transform infrared (FT-IR) data were collected on Perkin-Elmer Spectrum One FT-IR spectrometer using the corresponding KBr Pellets in the wavenumber range of 4000-400 cm⁻¹. The powder X-ray diffraction (PXRD) measurements were carried out on a Rigaku D/max 2500v/pc diffractometer equipped with Cu-K α radiation ($\lambda = 1.5418 \text{ \AA}$) at 40 kV and 40 mA, with a step size of 0.02° in 2θ and a scan speed of 5° min⁻¹. Elemental analyses for C, H, and N were performed on an Elementar Micro cube C, H, N elemental analyzer. The TG analyses (30-1000 °C) for **1** was conducted on a PerkinElmer Diamond TG/DTA thermal analyzer in a flowing nitrogen atmosphere with a heating rate of 5 °C min⁻¹. All magnetic data were measured on a Quantum Design MPMS SQUID-XL-7 SQUID magnetometer furnished with a 7 T magnet. The magnetic data of the two complexes were corrected with a consideration of diamagnetic contribution from the sample and the sample holder.

Single-crystal X-ray crystallography

Diffraction data for **1** were collected on a Bruker SMART CCD diffractometer (Mo K α radiation and $\lambda = 0.71073 \text{ \AA}$) in Φ and ω scan modes. The structures were solved by direct methods, followed by difference Fourier syntheses, and then refined by full-matrix least-squares techniques on F² using SHELXL. All other non-hydrogen atoms were refined with anisotropic thermal parameters. Some O atoms have a little large equivalent isotropic displacement parameters probably due to some unresolved disorder. Hydrogen atoms were placed at calculated positions and isotropically refined using a riding model. Some

uncoordinated OH groups from $(HL)^{3-}$ ligands, as well as some uncoordinated acetonitrile and water molecules, are modelled as disorder. Table S8 summarizes X-ray crystallographic data and refinement details for the complexes. Full details can be found in the CIF files provided in the Supporting Information. The CCDC reference number is 2223068 for **1**.

ESI-MS measurement.

ESI-MS measurements were conducted at a capillary temperature of 275 °C. Aliquots of the solution were injected into the device at 0.3 mL/h. The mass spectrometer used for the measurements was a Thermo Exactive, and the data were collected in positive and negative ion modes. The spectrometer was previously calibrated with the standard tune mix to give a precision of ca. 2 ppm within the region of 200-2000 m/z. The capillary voltage was 50 V, the tube lens voltage was 150 V, and the skimmer voltage was 25 V. The in-source energy was set within the range of 0-80 eV with a gas flow rate at 10% of the maximum.

The phase purity of cluster **1** was confirmed by PXRD measurements, which exhibited good agreement between experimental patterns and the simulated ones from single crystal X-ray diffraction data, respectively (Figure S2). Good thermal stability of the cluster was confirmed via the thermogravimetric analysis (TGA). For as-synthesized sample of the cluster, TGA curve exhibits a weight loss of 4.75% before 112 °C, which belongs to the loss of five EtOH molecules and six CH₃CN molecules (calculated 5.32%). With the temperature increasing, the skeleton remains stable in the range of 112 °C – 281°C, and then the structure of **1** start to decompose above 281°C. (Figure S3).

2. Continuous shape measure calculation results for Dy(III) ions

Table S1. SHAPE analysis of Dy1 in 1

Configuration	ABOXIY
Enneagon (D_{9h})	32.053
Octagonal pyramid (C_{8v})	22.747
Heptagonal bipyramid (D_{7h})	20.163
Johnson triangular cupola J3 (C_{3v})	15.161
Capped cube J8 (C_{4v})	8.538
Spherical-relaxed capped cube (C_{4v})	8.699
Capped square antiprism J10 (C_{4v})	0.858
Spherical capped square antiprism (C_{4v})	1.169
Tricapped trigonal prism J51 (D_{3h})	1.454
Spherical tricapped trigonal prism (D_{3h})	1.796
Tridiminished icosahedron J63 (C_{3v})	12.649
Hula-hoop (C_{2v})	11.836
Muffin (Cs)	1.993

Table S2. SHAPE analysis of Dy2 in 1

Configuration	ABOXIY
Octagon (D_{8h})	24.993
Heptagonal pyramid (C_{7v})	23.210
Hexagonal bipyramid (D_{6h})	17.828
Cube (O_h)	13.008
Square antiprism (D_{4d})	1.682
Triangular dodecahedron (D_{2d})	2.418
Johnson gyrobifastigium J26 (D_{2d})	14.022
Johnson elongated triangular bipyramid J14 (D_{3h})	28.128
Biaugmented trigonal prism J50 (C_{2v})	1.935
Biaugmented trigonal prism (C_{2v})	1.200
Snub diphenoïd J84 (D_{2d})	4.173
Triakis tetrahedron (T_d)	13.755
Elongated trigonal bipyramid (D_{3h})	23.200

Table S3. SHAPE analysis of Dy3 in **1**

Configuration	ABOXIY
Octagon (D_{8h})	29.762
Heptagonal pyramid (C_{7v})	22.562
Hexagonal bipyramid (D_{6h})	13.918
Cube (O_h)	7.959
Square antiprism (D_{4d})	1.295
Triangular dodecahedron (D_{2d})	1.204,
Johnson gyrobifastigium J26 (D_{2d})	14.642
Johnson elongated triangular bipyramid J14 (D_{3h})	26.793
Biaugmented trigonal prism J50 (C_{2v})	2.196
Biaugmented trigonal prism (C_{2v})	1.883
Snub diphenoïd J84 (D_{2d})	4.063
Triakis tetrahedron (T_d)	8.729
Elongated trigonal bipyramid (D_{3h})	22.005

Table S4. SHAPE analysis of Dy4 in **1**

Configuration	ABOXIY
Octagon (D_{8h})	28.965
Heptagonal pyramid (C_{7v})	22.673
Hexagonal bipyramid (D_{6h})	14.189
Cube (O_h)	8.250
Square antiprism (D_{4d})	1.058
Triangular dodecahedron (D_{2d})	1.628
Johnson gyrobifastigium J26 (D_{2d})	14.588
Johnson elongated triangular bipyramid J14 (D_{3h})	26.813
Biaugmented trigonal prism J50 (C_{2v})	2.272
Biaugmented trigonal prism (C_{2v})	2.030
Snub diphenoïd J84 (D_{2d})	4.355
Triakis tetrahedron (T_d)	9.064
Elongated trigonal bipyramid (D_{3h})	22.090

Table S5. SHAPE analysis of Dy5 in **1**

Configuration	ABOXIY
Heptagon (D_{7h})	26.150
Hexagonal pyramid (C_{6v})	20.645
Pentagonal bipyramid (D_{5h})	7.324
Capped octahedron (C_{3v})	3.024
Capped trigonal prism (C_{2v})	0.741
Johnson pentagonal bipyramid J13 (D_{5h})	9.914
Johnson elongated triangular pyramid J7 (C_{3v})	20.391

Table S6. SHAPE analysis of Dy6 in **1**

Configuration	ABOXIY
Octagon (D_{8h})	31.681
Heptagonal pyramid (C_{7v})	22.025
Hexagonal bipyramid (D_{6h})	15.459
Cube (O_h)	11.562
Square antiprism (D_{4d})	2.777
Triangular dodecahedron (D_{2d})	2.012
Johnson gyrobifastigium J26 (D_{2d})	13.970
Johnson elongated triangular bipyramid J14 (D_{3h})	27.879
Biaugmented trigonal prism J50 (C_{2v})	2.879
Biaugmented trigonal prism (C_{2v})	2.300
Snub diphenoïd J84 (D_{2d})	3.985
Triakis tetrahedron (T_d)	12.141
Elongated trigonal bipyramid (D_{3h})	24.054

Table S7. SHAPE analysis of Dy7 in **1**

Configuration	ABOXIY
Heptagon (D_{7h})	31.746
Hexagonal pyramid (C_{6v})	23.845
Pentagonal bipyramid (D_{5h})	0.759
Capped octahedron (C_{3v})	7.759
Capped trigonal prism (C_{2v})	6.218
Johnson pentagonal bipyramid J13 (D_{5h})	3.509
Johnson elongated triangular pyramid J7 (C_{3v})	23.199

3. Crystallographic data, bond distances and angles

Table S8. Crystallographic data of the cluster.

Cluster	1
Formula	C ₂₆₆ H ₃₇₇ Cu ₁₂ Dy ₁₄ N ₃₀ O _{119.5}
fw	8944.43
T / K	103(2)
λ / Å	1.54184
crystal system	triclinic
space group	P $\bar{1}$
a / Å	18.1682(2)
b / Å	21.1150(2)
c / Å	23.7150(3)
α / °	90.1080(10)
β / °	109.6270(10)
γ / °	106.6490(10)
V / Å ³	8161.10(17)
Z	1
D _c / g·cm ⁻³	1.820
μ / mm ⁻¹	18.369
2θ / °	5.422 to 130.018
F(000)	4411.0
reflns collected	126165
reflns unique	27220
R _{int}	0.0667
GOF on F ²	1.018
R ₁ (I > 2σ(I))	0.0555
ωR ₂ (I > 2σ(I))	0.1448
R ₁ (all data)	0.0609
ωR ₂ (all data)	0.1500

Table S9. Selected bond lengths / Å and bond angles / ° for **1**.

Dy1-O1	2.8545 (4)	Dy2-O1	2.2797 (3)	Dy3-O12A	2.370 (4)
Dy1-O2	2.379 (4)	Dy2-O2	2.372 (4)	Dy3-O14	2.281 (4)
Dy1-O3	2.351 (4)	Dy2-O3	2.368 (4)	Dy3-O56	2.298 (4)
Dy1-O5	2.475 (4)	Dy2-N2	2.502 (5)	Dy3-O19	2.460 (4)
Dy1-O9	2.350 (4)	Dy2-O13	2.310 (4)	Dy3-O20	2.408 (4)
Dy1-O11	2.345 (4)	Dy2-O14	2.329 (4)	Dy3-O37	2.389 (4)
Dy1-O56A	2.386 (4)	Dy2-O56	2.373 (4)	Dy3-O38	2.404 (4)
Dy1-O17A	2.367 (4)	Dy2-O17	2.346 (4)	Dy6-O34	2.268 (5)
Dy1-O19A	2.462 (4)	Dy5-O22	2.392 (4)	Dy6-O36	2.343 (6)
Dy4-O2	2.284 (4)	Dy5-H22	2.5561	Dy6-O38	2.445 (4)
Dy4-O5	2.439 (4)	Dy5-O23	2.274 (5)	Dy6-H38	2.2075 (4)
Dy4-O6	2.421 (4)	Dy5-N6	2.250 (5)	Dy6-O40	2.442 (4)
Dy4-O10	2.365 (5)	Dy5-O32	2.354 (4)	Dy6-O41	2.295 (5)
Dy4-O13	2.290 (4)	Dy5-O34	2.334 (4)	Dy6-O45	2.261 (5)
Dy4-O22	2.358 (5)	Dy5-O37	2.354 (4)	Dy6-O48	2.445 (5)
Dy4-O23	2.422 (4)	Dy5-O38	2.334 (4)	Dy6-O49	2.604 (6)
Dy4-O25	2.447 (4)	Cu2-O17	1.946 (4)	Cu3-O23	1.984 (4)
Cu1-O3	1.933 (4)	Cu2-O18	1.906 (4)	Cu3-O24	1.897 (5)
Cu1-O4	1.889 (4)	Cu2-N3	1.920 (6)	Cu3-N4	1.916 (5)
Cu1-N1	1.918 (5)	Cu2-O19	1.970 (4)	Cu3-O25	1.990 (4)
Cu1-O5	1.966 (4)	Cu2-O17	1.946 (4)	Cu6-O41	1.931 (5)
Cu4-O37	1.993 (4)	Cu5-O27	1.939 (5)	Cu6-O44	1.890 (5)
Cu4-O39	1.885 (5)	Cu5-O28	1.905 (6)	Cu6-N8	1.920 (6)
Cu4-N7	1.930 (5)	Cu5-N5	1.940 (6)	Cu6-O45	1.915 (5)
Cu4-O40	1.977 (4)	Cu5-O29	1.918 (5)	O56A-Dy1-O19A	69.04(14)
O1-Dy1A	2.8545 (4)	O11-Dy1-O56A	84.45(14)	O11-Dy1-O5	72.97(15)
O1-Dy2A	2.2797 (3)	O9-Dy1-O56A	135.70(14)	O9-Dy1-O5	76.47(14)
O11-Dy1-O9	104.76(15)	O3-Dy1-O56A	80.57(14)	O3-Dy1-O5	68.73(14)
O11-Dy1-O3	74.97(15)	O17A-Dy1-O56A	73.77(14)	O17A-Dy1-O5	138.29(14)
O9-Dy1-O3	143.72(15)	O2-Dy1-O56A	118.69(14)	O2-Dy1-O5	67.91(13)
O11-Dy1-O17A	142.93(15)	O11-Dy1-O19A	75.33(15)	O56A-Dy1-O5	145.50(13)
O9-Dy1-O17A	73.69(15)	O9-Dy1-O19A	71.70(14)	O19A-Dy1-O5	126.75(14)
O3-Dy1-O17A	128.33(14)	O3-Dy1-O19A	139.03(14)	O11-Dy1-O1	128.23(11)
O11-Dy1-O2	136.38(15)	O17A-Dy1-O19A	69.03(14)	O9-Dy1-O1	127.00(11)
O9-Dy1-O2	84.37(14)	O2-Dy1-O19A	145.43(13)	O2-Dy2-O56	87.46(14)
O3-Dy1-O2	73.52(14)	O3-Dy1-O1	64.08(10)	O1-Dy2-N2	137.44(12)
O17A-Dy1-O2	80.69(14)	O17A-Dy1-O1	64.25(10)	O13-Dy2-N2	68.85(16)
O1-Dy2-O13	136.12(11)	O2-Dy1-O1	59.06(9)	O14-Dy2-N2	68.28(16)
O1-Dy2-O14	136.62(10)	O56A-Dy1-O1	59.62(10)	O17-Dy2-N2	78.83(16)

O13-Dy2-O14	80.17(16)	O19A-Dy1-O1	117.31(10)	O3-Dy2-N2	79.61(16)
O1-Dy2-O17	74.72(10)	O5-Dy1-O1	115.93(10)	O2-Dy2-N2	133.73(16)
O13-Dy2-O17	146.64(15)	O1-Dy2-O2	68.31(9)	O56-Dy2-N2	133.57(16)
O14-Dy2-O17	80.44(15)	O13-Dy2-O2	70.32(14)	O14-Dy3-O56	72.52(14)
O1-Dy2-O3	73.89(10)	O14-Dy2-O2	124.18(14)	O14-Dy3-O12A	150.68(15)
O13-Dy2-O3	80.96(15)	O17-Dy2-O2	142.66(14)	O56-Dy3-O12A	84.17(14)
O14-Dy2-O3	146.90(14)	O3-Dy2-O2	73.34(14)	O14-Dy3-O37	116.85(15)
O17-Dy2-O3	101.62(14)	O1-Dy2-O56	69.03(10)	O56-Dy3-O37	76.67(14)
O14-Dy3-O20	84.31(15)	O13-Dy2-O56	123.05(15)	O12A-Dy3-O37	73.00(15)
O56-Dy3-O20	138.25(15)	O14-Dy2-O56	70.34(14)	O14-Dy3-O38	76.21(15)
O12A-Dy3-O20	102.72(16)	O17-Dy2-O56	74.42(14)	O56-Dy3-O38	113.34(15)
O37-Dy3-O20	144.95(15)	O3-Dy2-O56	142.44(14)	O12A-Dy3-O38	130.73(14)
O38-Dy3-O20	93.31(15)	O20-Dy3-O40	75.52(15)	O37-Dy3-O38	67.73(14)
O14-Dy3-O40	136.18(14)	O14-Dy3-O19	80.43(15)	O2-Dy4-O13	72.24(14)
O56-Dy3-O40	143.62(14)	O56-Dy3-O19	70.47(14)	O2-Dy4-O22	115.04(15)
O12A-Dy3-O40	72.70(14)	O12A-Dy3-O19	75.07(14)	O13-Dy4-O22	76.63(16)
O37-Dy3-O40	69.98(14)	O37-Dy3-O19	135.86(14)	O2-Dy4-O10	82.98(15)
O38-Dy3-O40	66.79(14)	O38-Dy3-O19	153.43(14)	O13-Dy4-O10	150.66(15)
O2-Dy4-O23	75.18(14)	O20-Dy3-O19	71.78(15)	O22-Dy4-O10	129.54(15)
O13-Dy4-O23	113.27(15)	O40-Dy3-O19	126.83(14)	O2-Dy4-O6	138.01(15)
O22-Dy4-O23	67.27(15)	O23-Dy4-O5	136.61(14)	O13-Dy4-O6	83.07(15)
O10-Dy4-O23	73.73(15)	O2-Dy4-O25	141.16(14)	O22-Dy4-O6	90.52(16)
O6-Dy4-O23	146.76(14)	O13-Dy4-O25	138.29(15)	O10-Dy4-O6	106.66(16)
O2-Dy4-O5	69.99(14)	O22-Dy4-O25	66.56(15)	O34-Dy5-O32	86.82(19)
O13-Dy4-O5	79.86(15)	O10-Dy4-O25	71.00(15)	O34-Dy5-O23	152.17(16)
O22-Dy4-O5	152.54(15)	O6-Dy4-O25	78.47(15)	O32-Dy5-O23	79.47(18)
O10-Dy4-O5	77.03(14)	O23-Dy4-O25	70.22(14)	O34-Dy5-O38	75.53(16)
O6-Dy4-O5	72.63(15)	O5-Dy4-O25	127.89(14)	O32-Dy5-O38	135.12(18)
O45-Dy6-O34	84.00(18)	O34-Dy5-N6	69.40(18)	O23-Dy5-O38	130.51(14)
O45-Dy6-O41	68.78(17)	O32-Dy5-N6	68.29(19)	O34-Dy5-O37	81.14(17)
O34-Dy6-O41	94.59(18)	O23-Dy5-N6	83.00(16)	O32-Dy5-O37	148.39(17)
O45-Dy6-O36	79.13(19)	O38-Dy5-N6	136.42(17)	O23-Dy5-O37	98.07(14)
O34-Dy6-O36	98.9(2)	O37-Dy5-N6	80.11(17)	O38-Dy5-O37	69.48(15)
O41-Dy6-O36	143.57(19)	O22-Dy5-N6	137.47(17)	O34-Dy5-O22	131.55(17)
O45-Dy6-O40	141.71(17)	O45-Dy6-O38	142.44(16)	O32-Dy5-O22	75.91(17)
O34-Dy6-O40	84.49(16)	O34-Dy6-O38	73.01(15)	O23-Dy5-O22	68.24(15)
O41-Dy6-O40	75.93(15)	O41-Dy6-O38	140.75(15)	O38-Dy5-O22	85.54(15)
O36-Dy6-O40	138.82(17)	O36-Dy6-O38	75.68(18)	O50-Dy7-O29	101.4(4)
O45-Dy6-O48	127.67(18)	O40-Dy6-O38	66.07(14)	O50-Dy7-O32	167.9(4)
O34-Dy6-O48	147.41(16)	O48-Dy6-O38	75.83(15)	O29-Dy7-O32	90.07(19)
O41-Dy6-O48	103.64(18)	O45-Dy6-O49	77.75(19)	O50-Dy7-O35	101.5(3)
O36-Dy6-O48	82.31(19)	O34-Dy6-O49	161.48(18)	O29-Dy7-O35	78.7(2)
O40-Dy6-O48	74.31(15)	O41-Dy6-O49	76.0(2)	O32-Dy7-O35	76.8(2)

O35-Dy7-O27	145.1(2)	O36-Dy6-O49	80.9(2)	O50-Dy7-O27	97.1(3)
O50-Dy7-O25	89.2(3)	O40-Dy6-O49	108.04(18)	O29-Dy7-O27	68.73(18)
O29-Dy7-O25	144.83(18)	O48-Dy6-O49	51.09(17)	O32-Dy7-O27	90.68(19)
O32-Dy7-O25	83.44(18)	O38-Dy6-O49	124.17(17)	O50-Dy7-O29	101.4(4)
O35-Dy7-O25	132.26(19)	O35-Dy7-O22	66.75(19)	O29-Dy7-O22	144.65(17)
O27-Dy7-O25	76.79(16)	O27-Dy7-O22	141.62(17)	O32-Dy7-O22	75.33(16)
O50-Dy7-O22	92.9(4)	O25-Dy7-O22	66.34(15)	O24-Cu3-O23	92.24(19)
O4-Cu1-N1	93.3(2)	O18-Cu2-N3	92.1(2)	N4-Cu3-O23	170.2(2)
O4-Cu1-O3	92.32(18)	O18-Cu2-O17	93.88(19)	O24-Cu3-O25	174.5(2)
N1-Cu1-O3	171.7(2)	N3-Cu2-O17	173.4(2)	N4-Cu3-O25	85.2(2)
O4-Cu1-O5	175.1(2)	O18-Cu2-O19	176.0(2)	O23-Cu3-O25	89.62(18)
N1-Cu1-O5	86.3(2)	N3-Cu2-O19	85.4(2)	O44-Cu6-O45	175.9(2)
O3-Cu1-O5	88.70(18)	O17-Cu2-O19	88.71(17)	O44-Cu6-N8	93.7(2)
O39-Cu4-N7	93.6(2)	O28-Cu5-O29	172.4(3)	O45-Cu6-N8	85.8(2)
O39-Cu4-O40	174.7(2)	O28-Cu5-O27	99.2(2)	O44-Cu6-O41	96.9(2)
N7-Cu4-O40	84.8(2)	O29-Cu5-O27	83.9(2)	O45-Cu6-O41	84.0(2)
O39-Cu4-O37	93.71(19)	O28-Cu5-N5	92.5(2)	N8-Cu6-O41	168.4(2)
N7-Cu4-O37	170.7(2)	O29-Cu5-N5	85.0(2)	O27-Cu5-N5	167.4(2)
O40-Cu4-O37	88.38(18)				

Symmetry code: (A) $-x+1, -y+2, -z+1$.

4. IR, PXRD and TG figures of 1

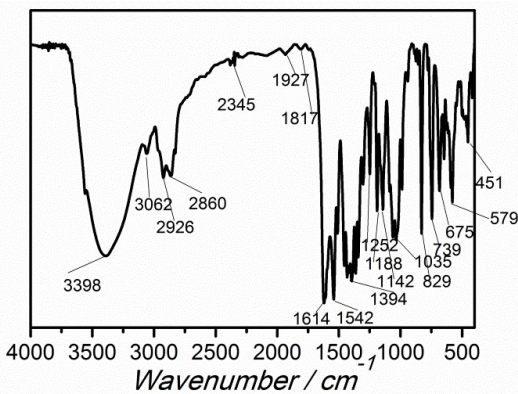


Figure S1. FT-IR spectrum of **1**.

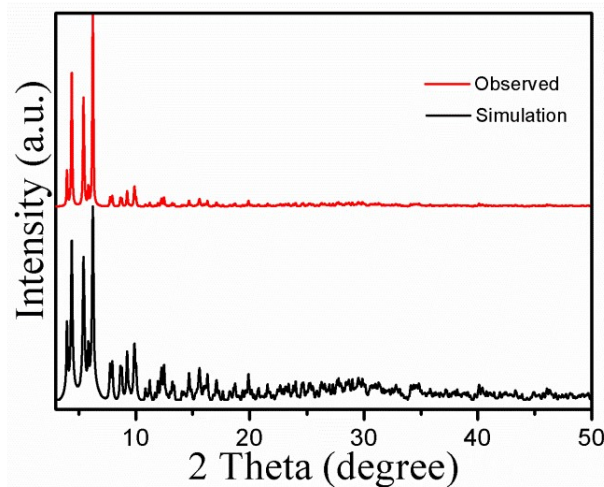


Figure S2. PXRD patterns of **1**.

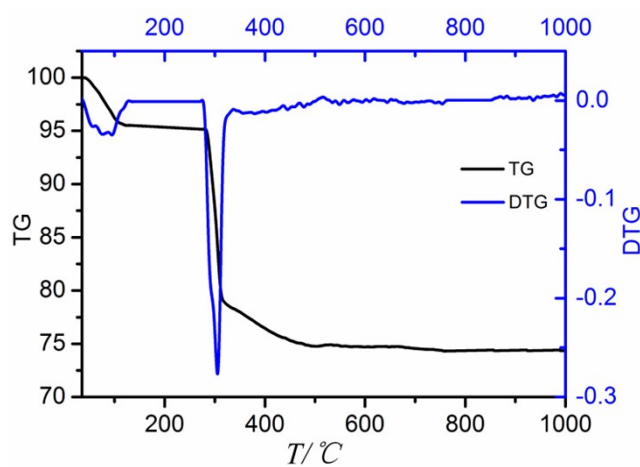


Figure S3. TG patterns of **1**.

5. Additional structural figures of 1

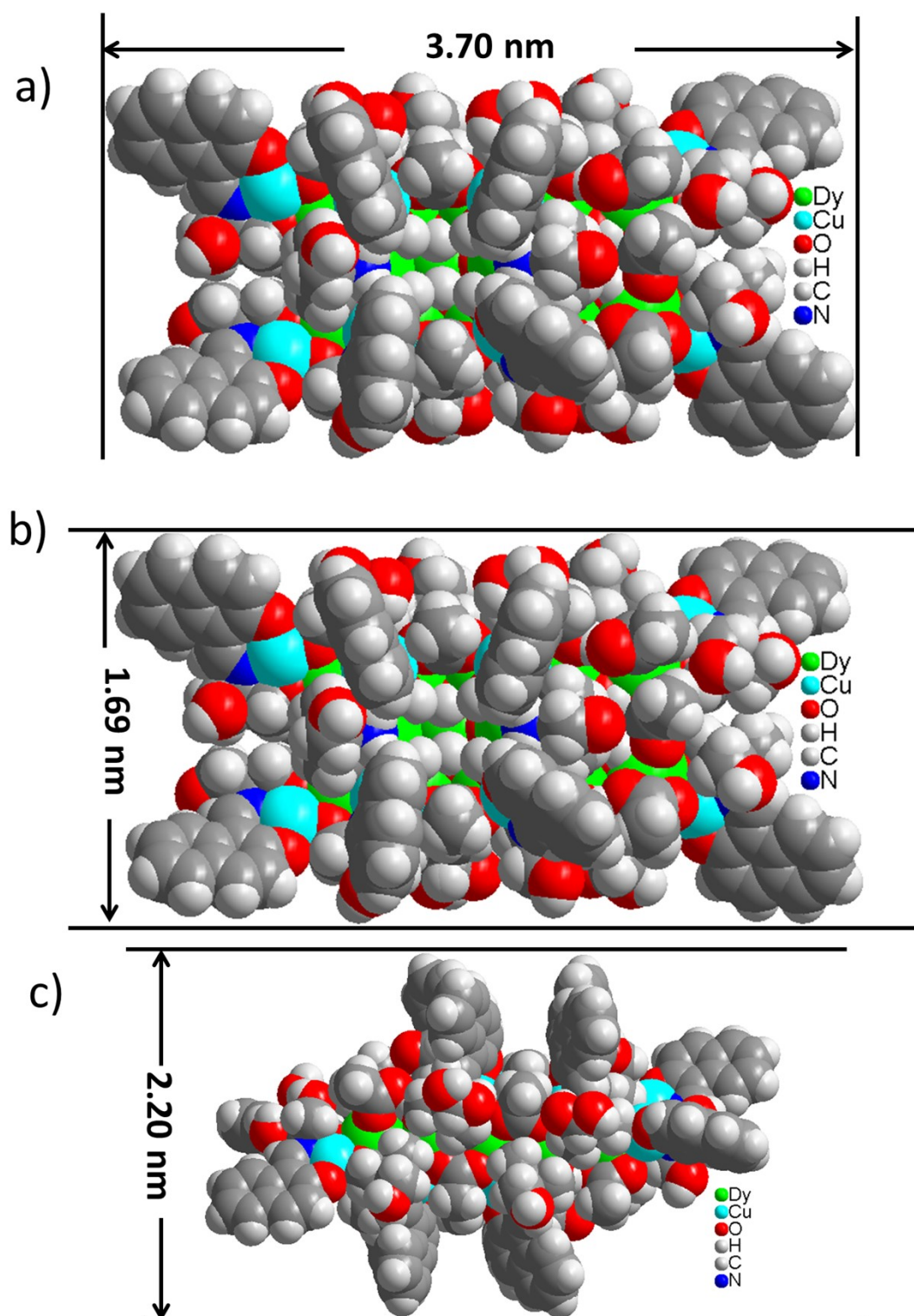


Figure S4. The size of cluster 1.

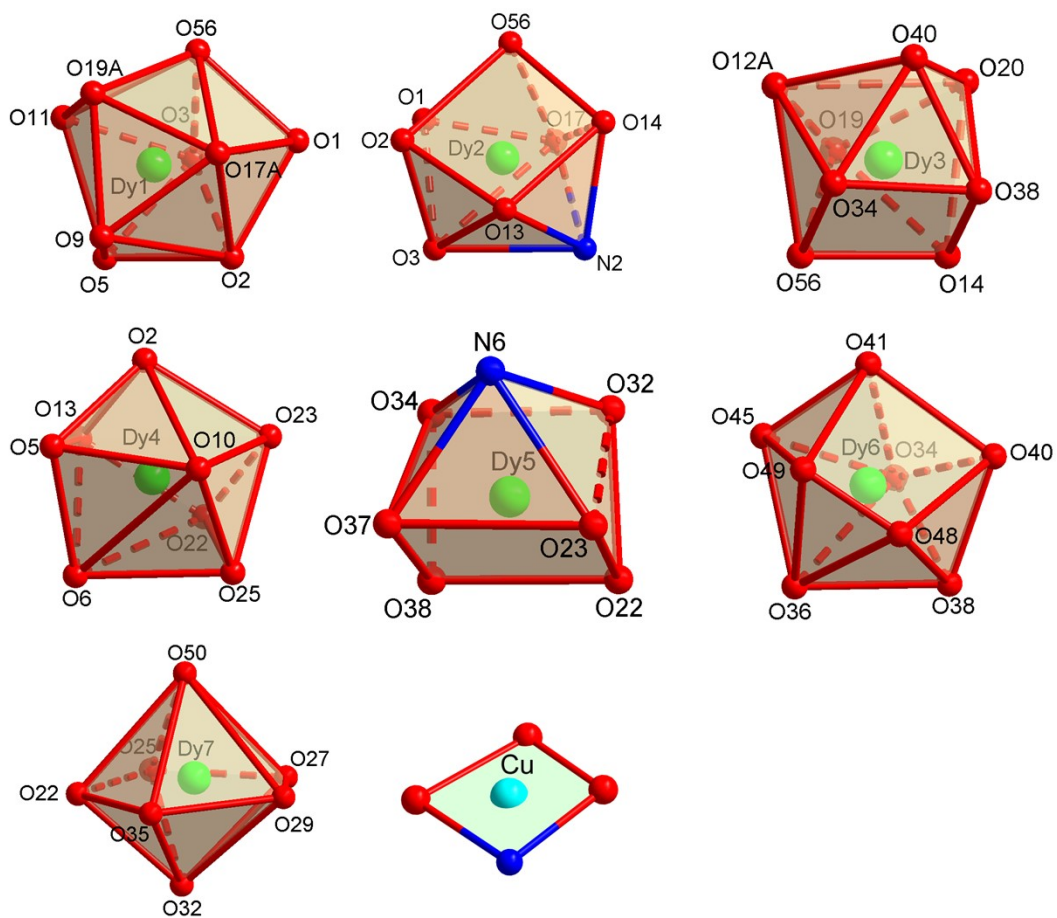


Figure S5. Coordination polyhedrons around the Dy(III) ions and Cu(II) of **1** with labels for selected atoms.

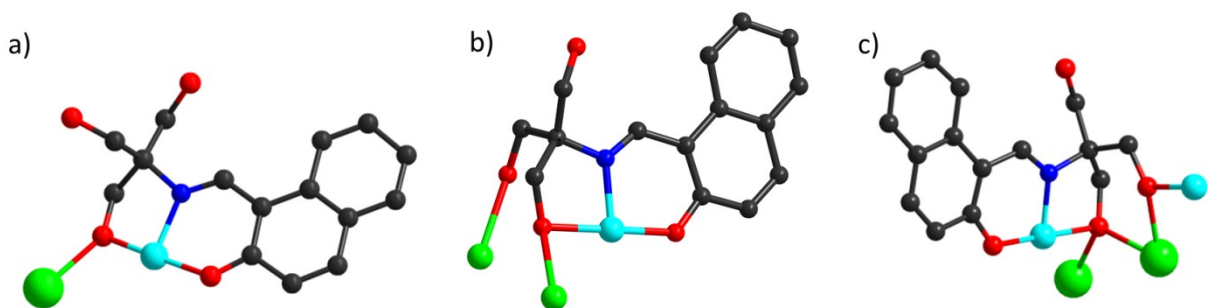


Figure S6. Different bridging modes of $(\text{H}_2\text{L})^{2-}$ (a and b) and $(\text{HL})^{3-}$ (c) in **1**.

6. Major species and fragments detected in 1

Table S10. Major species and fragments detected in the formation reaction for **1** through HRESI-MS.

Symbol of intermediates	1 (In-Source CID 0 eV)		
	Peaks	<i>Obs. m/z</i>	<i>Calc. m/z</i>
Dy	[Dy(NO ₃) ₂] ⁺	287.92	287.90
DyL'	[Dy(H ₂ L')(NO ₃)(H ₂ O)(CH ₃ OH)] ⁺	411.88	412.01
DyCuL	[DyCu(H ₂ L)(CH ₃ CN)(OAc) ₂] ⁺	600.07	600.00
Dy ₂ CuL	[Dy ₂ Cu(L)(OH) ₂ (NO ₃)(H ₂ O) ₄ (CH ₃ OH) ₂ (CH ₃ CH ₂ OH)] ⁺	957.94	957.90
DyCu ₂ L	[DyCu ₂ (HL)(OAc)(OH) ₂ (CH ₃ CH ₂ OH)(CH ₃ OH)(H ₂ O)] ⁺	752.99	752.99
	[DyCu ₂ (HL)(NO ₃)(OH) ₂ (CH ₃ CH ₂ OH)(CH ₃ OH)(H ₂ O) ₂] ⁺	771.94	771.96
	[DyCu ₂ (HL)(NO ₃)(OH) ₂ (CH ₃ CN)(CH ₃ OH)(H ₂ O) ₃] ⁺	785.91	785.97
Dy ₂ Cu ₂ L ₂	[Dy ₂ Cu ₂ (L)(HL)(OAc) ₂] ⁺	1105.06	1104.94
	[Dy ₂ Cu ₂ (L) ₂ (OAc) ₂] ⁺	1119.99	1119.87
	[Dy ₂ Cu ₂ (L)(HL)(OAc)(NO ₃)(CH ₃ CN) ₂ (CH ₃ OH)] ⁺	1231.97	1231.98
	[Dy ₂ Cu ₂ (L)(HL)(OAc)(NO ₃)(CH ₃ CN) ₄ (CH ₃ OH) ₂ (H ₂ O)] ⁺	1361.99	1362.06
	[Dy ₂ Cu ₂ (L)(HL)(OAc)(NO ₃)(CH ₃ CN) ₃ (CH ₃ OH) ₃ (H ₂ O) ₃] ⁺	1390.94	1391.09
Dy ₂ Cu ₃ L ₄	[Dy ₂ Cu ₃ (H ₃ L)(H ₂ L) ₃ (OAc) ₃ (NO ₃) ₂ (HO) ₃ (CH ₃ OH) ₃] ⁺	1790.93	1791.10
	[Dy ₂ Cu ₃ (H ₂ L) ₂ (H ₂ L) ₂ (OAc) ₄ (NO ₃) ₃ (HO) ₂ (CH ₃ OH) ₄] ⁺	1802.79	1803.15
Dy ₃ Cu ₂ L ₂	[Dy ₃ Cu ₂ (L) ₂ (OAc)(NO ₃)(OH) ₂ (CH ₃ CH ₂ OH) ₂ (HO)] ⁺	1423.92	1423.93
	[Dy ₃ Cu ₂ (L) ₂ (OAc)(NO ₃)(OH) ₂ (CH ₃ CN) ₃ (CH ₃ OH)(CH ₃ CH ₂ OH)(H ₂ O)] ⁺	1454.87	1454.95
	[Dy ₃ Cu ₂ (L)(HL)(OAc) ₅ (H ₂ O)(CH ₃ OH)] ⁺	1506.03	1505.95
Dy ₃ Cu ₄ L ₄	[Dy ₃ Cu ₄ (H ₂ L) ₄ (OAc) ₆ (NO ₃)(CH ₃ OH) ₃] ⁺	2350.83	2351.08
	[Dy ₃ Cu ₄ (H ₂ L) ₃ (H ₂ L)(OAc) ₆ (NO ₃)(CH ₃ OH) ₃ (HO)] ⁺	2400.94	2401.12
Dy ₄ Cu ₃ L ₂	[Dy ₄ Cu ₂ (L) ₂ (OAc) ₄ (NO ₃) ₂ (HO) ₄ (CH ₃ CN)] ⁺	1802.70	1802.86
Dy ₄ Cu ₃ L ₃	[Dy ₄ Cu ₃ (L) ₃ (OAc) ₄ (NO ₃)(HO) ₂ (CH ₃ OH)(CH ₃ CN)] ⁺	2064.93	2064.89
	[Dy ₄ Cu ₃ (L) ₃ (OAc) ₅ (HO) ₂ (CH ₃ OH) ₂ (CH ₃ CN)] ⁺	2076.80	2076.94
Dy ₅ Cu ₄ L ₄	[Dy ₅ Cu ₄ (L) ₄ (OAc) ₆ (NO ₃)(HO)(CH ₃ OH)] ⁺	2623.86	2623.85

Table S11. The change of the relative HRESI-MS (positive mode) peak intensities for the intermediate species with the reaction time in the formation reaction of **1**.

Reaction time	The relative HRESI-MS peak intensities for the intermediate species											
	Dy	DyL'	DyCuL	Dy ₂ CuL	DyCu ₂ L	Dy ₂ Cu ₂ L ₂	Dy ₃ Cu ₂ L ₂	Dy ₂ Cu ₃ L ₄	Dy ₄ Cu ₂ L ₂	Dy ₄ Cu ₃ L ₃	Dy ₃ Cu ₄ L ₄	Dy ₅ Cu ₄ L ₄
1 min	0.10	0.10	0.01	0.01	0.2	0.01	0.01	0	0	0	0	0
5 min	0.20	0.10	0.012	0.01	0.15	0.01	0.01	0	0	0	0	0
15 min	0.47	0.32	0.013	0.015	0.1	0.02	0.02	0	0	0	0	0
25 min	0.67	0.48	0.8	0.1	0.01	0.01	0.01	0	0	0	0	0
45 min	0.75	0.64	0.9	0.2	0.2	0.01	0.01	0	0	0	0	0
60 min	0.59	0.53	0.3	0.28	0.09	0.01	0.01	0	0	0	0	0
90 min	0.44	0.49	0.4	0.36	0.48	0.02	0.20	0.01	0.01	0.01	0	0
120 min	0.42	0.38	0.3	0.23	0.65	0.03	0.25	0.01	0.01	0.02	0	0
180 min	0.34	0.51	0.2	0.15	0.66	0.19	0.18	0.04	0.05	0.01	0.01	0
240 min	0.34	0.38	0.18	0.07	0.87	0.19	0.40	0.06	0.07	0.07	0.01	0
360 min	0.41	0.50	0.15	0.07	0.20	0.64	0.65	0.15	0.14	0.11	0.06	0
450 min	0.23	0.36	0.01	0.08	0.10	0.62	0.80	0.20	0.23	0.32	0.1	0
600 min	0.33	0.14	0.01	0.11	0.10	0.51	0.30	0.43	0.29	0.39	0.13	0.11
810 min	0.20	0.04	0.02	0.02	0.02	0.11	0.40	0.35	0.28	0.45	0.12	0.34
1080 min	0.04	0.01	0.01	0.043	0.06	0.30	0.3	0.17	0.24	0.29	0.15	0.34
1440 min	0.10	0.01	0.015	0.01	0.01	0.23	0.25	0.15	0.22	0.11	0.11	0.21

7. The superposed simulated and observed spectra of several species figure of 1

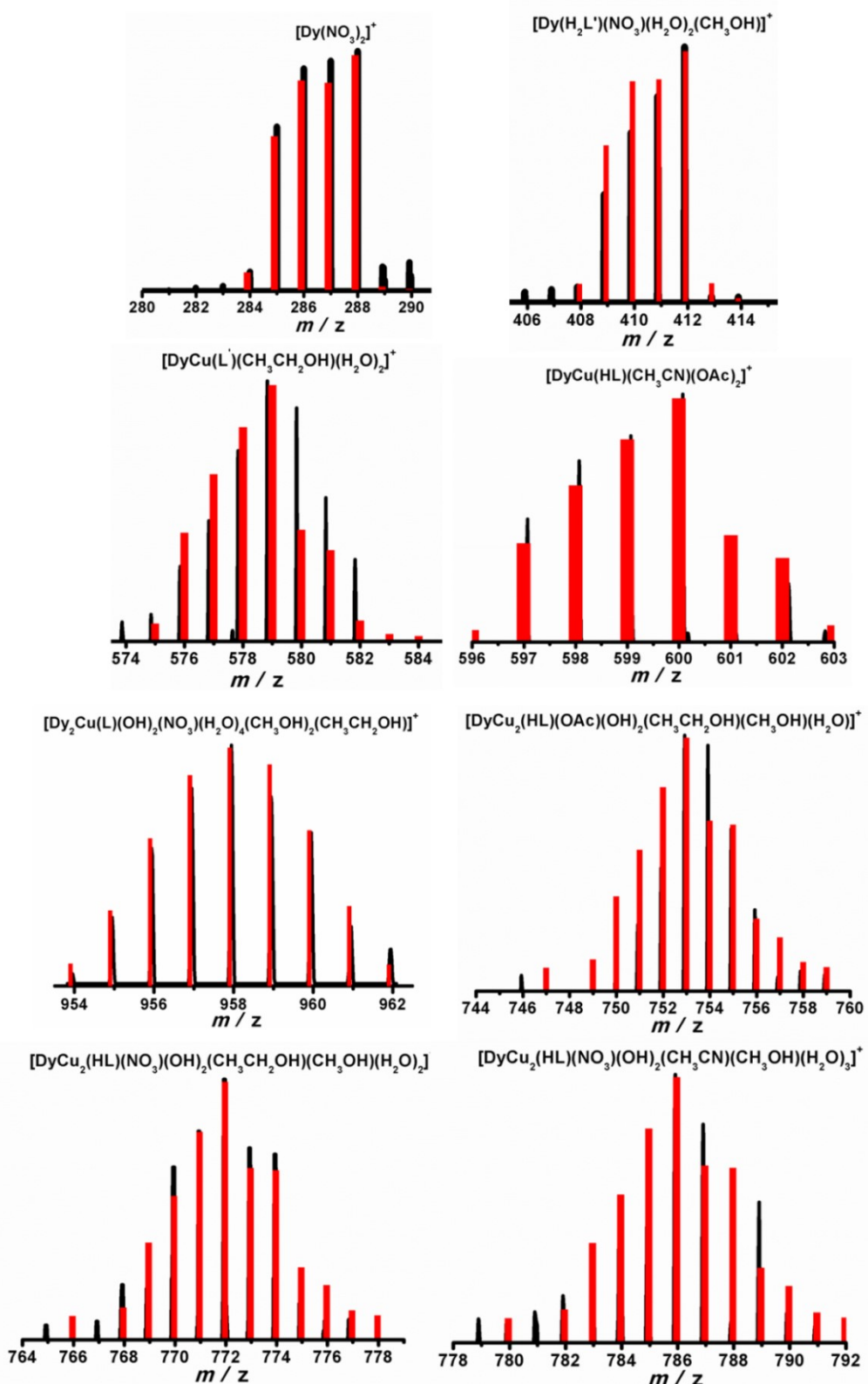


Figure S7. The superposed simulated (red) and observed (black) spectra of several species in the Time-dependent ESI-MS of **1**.

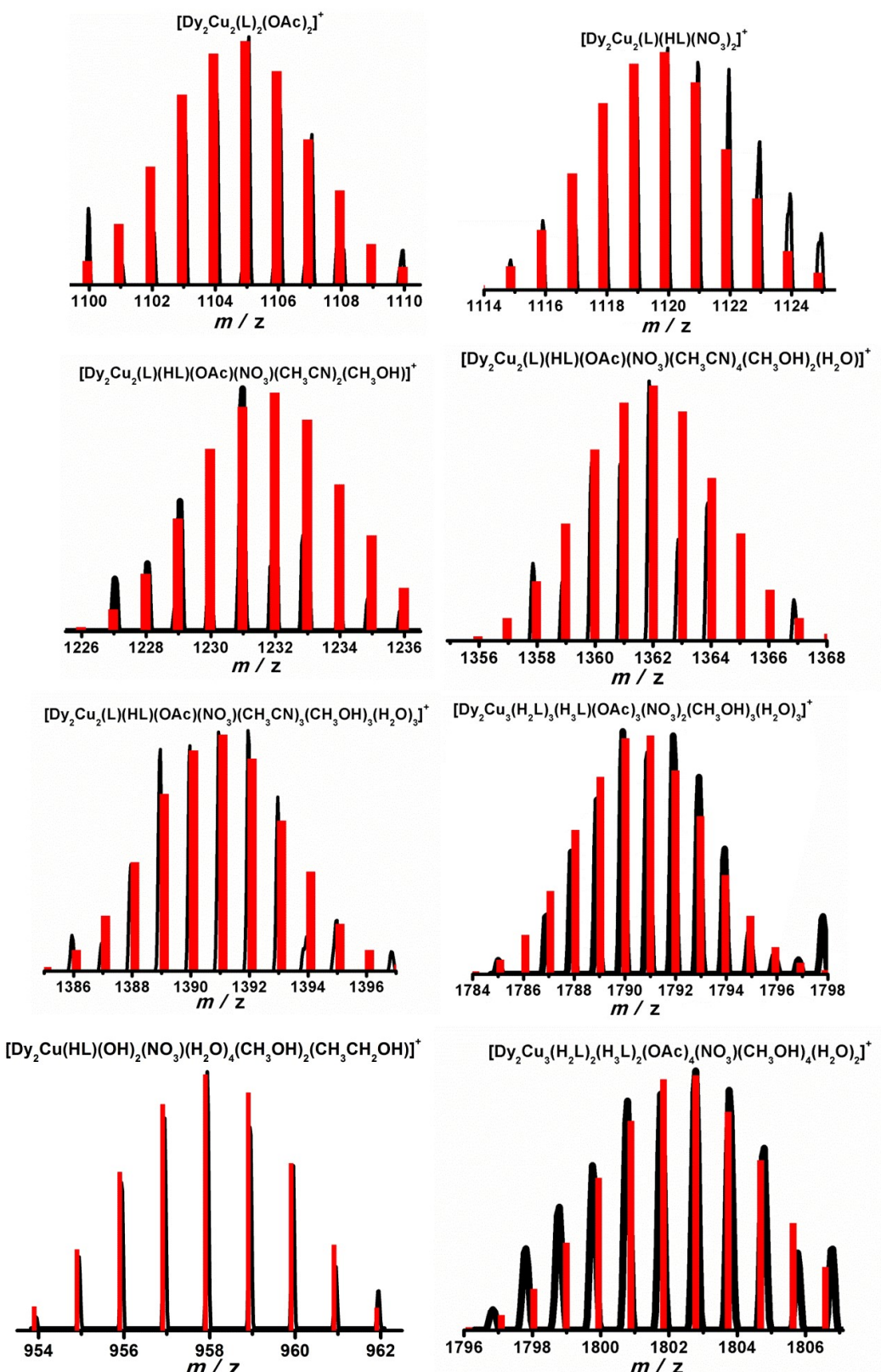


Figure S8. The superposed simulated (red) and observed (black) spectra of several species in the Time-dependent ESI-MS of **1**.

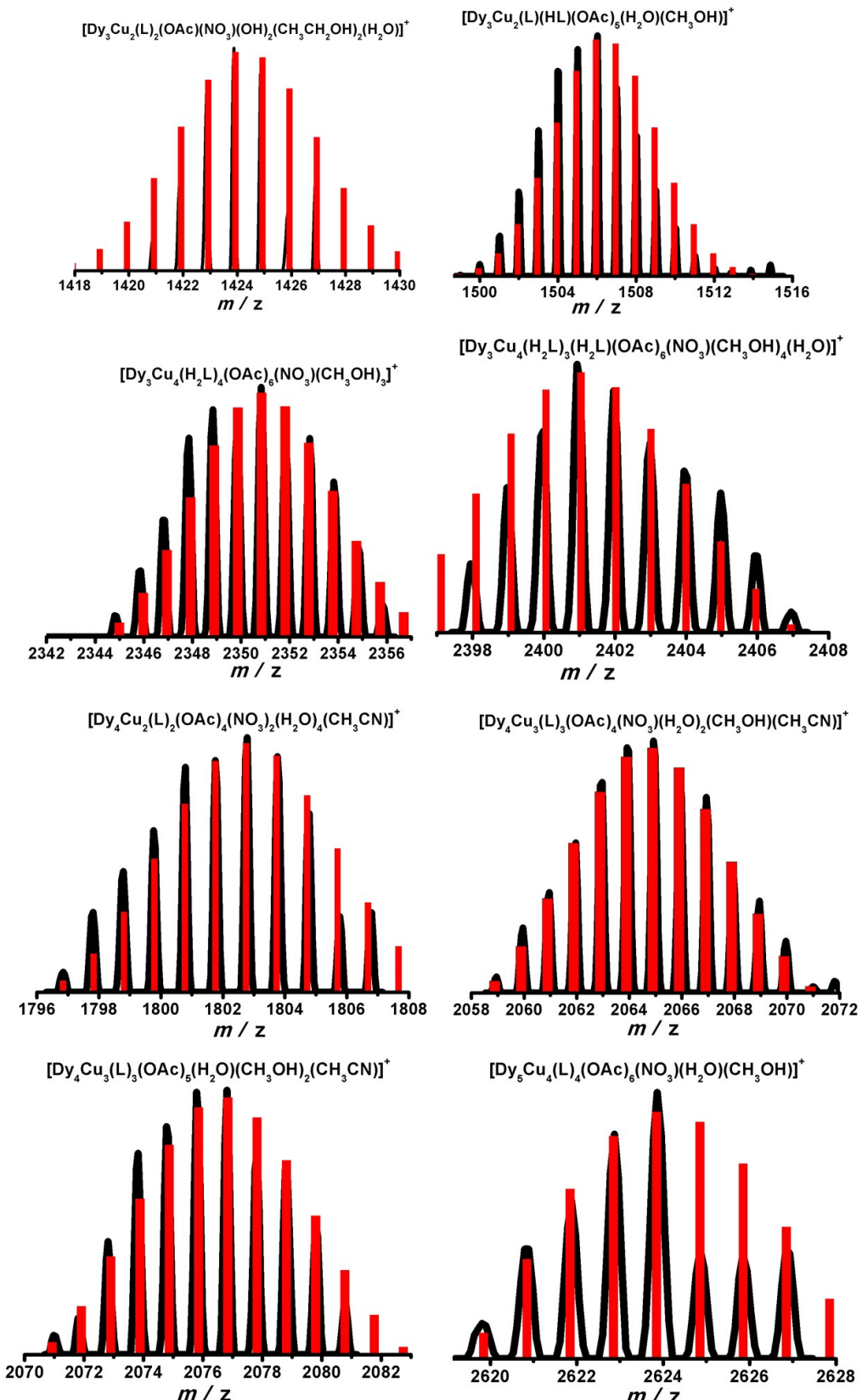


Figure S9. The superposed simulated (red) and observed (black) spectra of several species in the Time-dependent ESI-MS of 1.

8. Additional figures for static magnetic properties of **1**

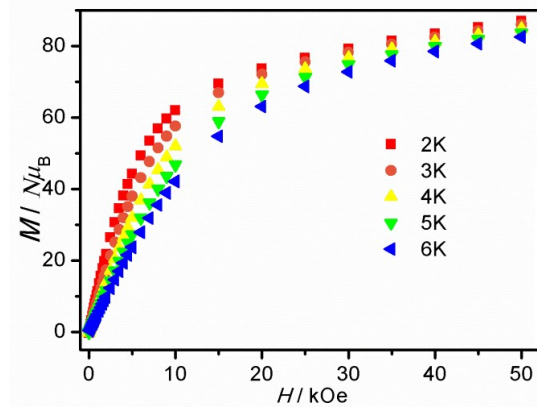


Figure S10. Plots of M vs. H for **1** measured at 2, 3, 4, 5 and 6 K.

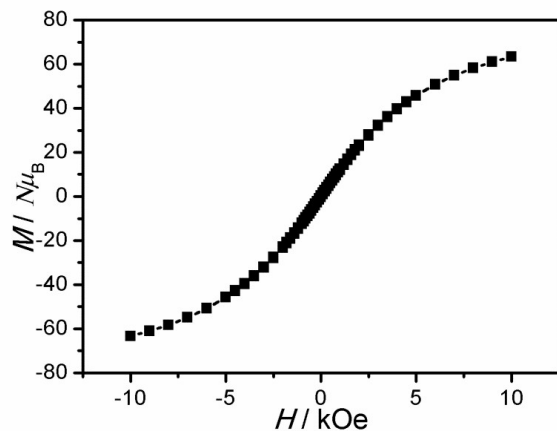


Figure S11. Plots of Magnetic hysteresis loops for **1**.

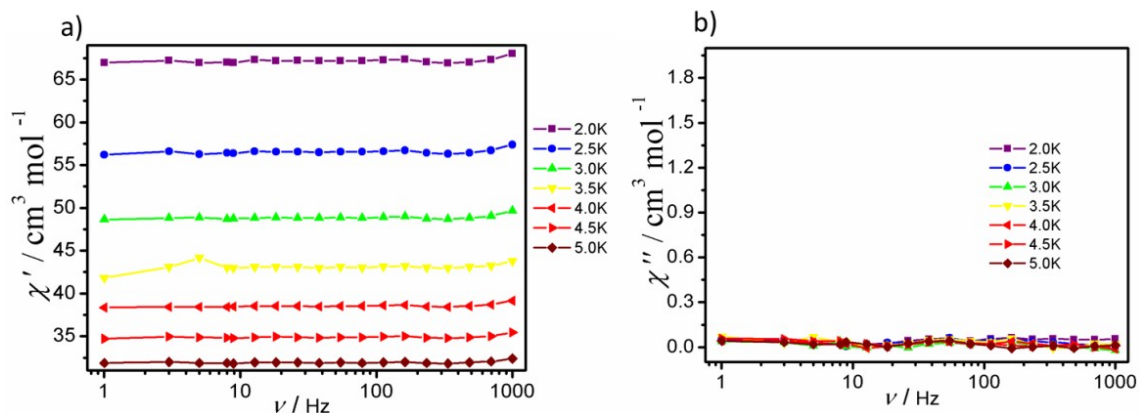


Figure S12. Plots of χ' vs ν (a) and χ'' vs ν (a) at 2.0 - 5.0 K under a dc field of 0 Oe for **1**.

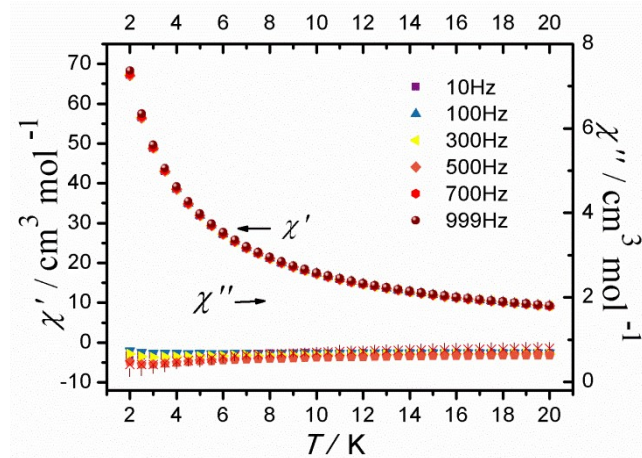


Figure S13 Temperature-dependent χ' and χ'' ac susceptibilities under zero dc field for **1**.

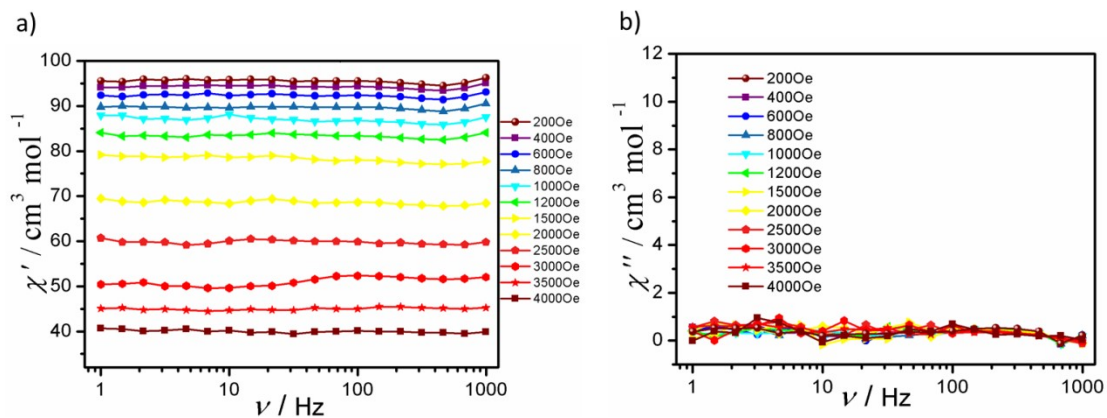


Figure S14. Plots of χ' and χ'' vs ν at 2 K under different dc field for **1**.